Journal of the Optical Society of Korea
Vol. 19, No. 2, April 2015, pp. 188-198

ISSN: 1226-4776(Print) / ISSN: 2093-6885(Online)
DOI: http://dx.doi.org/10.3807/JOSK.2015.19.2.188

Modified Airy Function Method Applied to Optical Waveguides and Quantum Tunneling: A Critical Analysis

Ki-Young Lee[1], Chul Han Kim[1], Dongwook Park[2], and Chang-Min Kim[1]*

[1]School of Electronics and Computer, University of Seoul, Seoul 130-743, Korea
[2]School of Electronic and Electrical Engineering, Hongik University, Seoul 121-791, Korea

(Received January 15, 2015 : revised March 25, 2015 : accepted March 26, 2015)

The validity of applying the Modified Airy Function (MAF) method to the problems of graded-index optical waveguides and graded potential barrier analysis was critically examined. In the former case, the method yielded very accurate results from the derived eigenvalue equations. In the latter case, however, the same method produced results that deviated significantly from exact numerical results for barriers with a smooth peak. The causes of the discrepancies were investigated in detail.

Keywords : MAF method, Graded profile, Waveguide analysis, Tunneling probability, WKB method
OCIS codes : (230.7370) Waveguides; (240.7040) Tunneling

I. INTRODUCTION

Analysis of optical devices such as waveguides and directional couplers is essential to be able to predict their characteristics, and involves solving the Helmholtz equation. Meanwhile, analysis of tunneling phenomena is necessary in various problems of particle physics, as well as in certain quantum devices, which requires solving the Schrödinger equation. Despite their apparent differences, the two problems are quite closely related from a theoretical standpoint, because the two equations are nearly identical in form. Whatever the structure, one must decide whether to employ a numerical method, or to rely on a mathematical approach for analysis. As to numerical methods for solving the wave equation, one may choose one of the well-known simulation techniques such as FEM (finite element method), BPM (beam propagation method), the TM (transfer matrix) method, and so on, depending on the given application. Numerical methods provide very accurate results, but not necessarily physical insight. On the other hand, mathematical approaches provide such insight, allowing closed-form solutions, but are limited in their use since exact solutions are available only for specific cases such as linear, exponential, and inverse hyperbolic cosine index profiles.

Thus, for a majority of graded structures, many have resorted to approximate mathematical methods. One of the most widely used methods for handling this class of problems is the WKB (Wentzel-Kramers-Brillouin) method. It is well known that results of this method tend to deviate from the exact solution on the whole since trial solutions diverge at the turning points [1]. Despite this deficiency the WKB method has frequently been employed by many researchers [2, 3] owing to the simple mathematical expressions involved, availability of eigenvalue equations in closed forms, and easy estimation of final results. In an effort to circumvent such inherent deficiency of the WKB method, Langer [4] proposed a method utilizing the Modified Airy functions (MAF), which was later applied to the analysis of optical waveguides and also to tunneling problems in connection with potential barriers by Ghatak et al. [5, 6]. More recently, Kim et al. applied the MAF method to a variety of optical waveguides [7, 8] and tunneling problems [9, 10] by employing MAFs in constructing the trial solution across the entire structure, demonstrating the method's accuracy. Despite these recent advances, however, researchers have failed to clearly point out that the method does not yield satisfactory results in cases where particle energy is comparable to the barrier peak, for some classes of potential barrier profiles, and have not provided a rational explanation for such behavior. This work aims to address these shortcomings.

This paper is comprised as follows. First, the basics of the MAF method are addressed, with an optical waveguide as the platform for discussion. A trial solution is presented

*Corresponding author: cmkim@uos.ac.kr

for each distinct region, followed by the corresponding 'connection formula'. Then actual application of the MAF technique to the analysis of graded-index waveguides is presented. Using the MAF trial solutions, a closed-form expression of the eigenvalue equation is derived for graded-waveguides. The eigenvalue equation is then solved for several graded-index profiles, to yield the dispersion curves. The results are shown to be in very good agreement with exact numerical results obtained using the FEM.

The second part comprises the analysis of the tunneling problem. Based on the same MAF trial solutions postulated in the waveguide case, tunneling probability is derived in matrix form and evaluated for a number of graded potential barriers. The results are compared with exact numerical solutions obtained using the TM method, whose accuracy has already been verified in numerous studies [11, 12]. It turns out that MAF method fails for profiles with a smooth peak and that the WKB method does not work as well for profiles with an abrupt truncation or change.

Possible causes for the discrepancy in accuracy of the results for waveguide and tunneling problems upon application of the same MAF method are investigated in a systematic manner. This evaluation has not been previously addressed, to our knowledge. In the process, the corresponding results of the conventional WKB method and the FEM or TM method – the latter two providing exact numerical solutions – are also presented for comparison.

II. MAF TRIAL SOLUTIONS AND CONNECTION FORMULAE

In this section, a brief overview of the MAF method is presented. Although the discussion is conducted for optical waveguides, the formulation and basic concepts apply equally to the potential-barrier problem.

Let us start with the one-dimensional wave equation for optical waveguides:

$$\frac{d^2\psi(x)}{dx^2}+\Gamma(x)\psi(x)=0 \tag{1}$$

where

$$\Gamma(x)\equiv k_0{}^2\left(n^2(x)-N^2\right) \tag{2}$$

In (2), $n(x)$ denotes the given index profile across the waveguide structure and N is the eigenvalue to be found, the mode index.

In Fig. 1 a diagram of $\Gamma(x)$ depicting the distinct regions according to the sign of $\Gamma(x)$ is presented for clarification of the quantities involved. In the $Q(x)$ region where $\Gamma(x)$ is positive, the solution is oscillatory, and in the $P(x)$ region the solution is either monotonically growing or decaying.

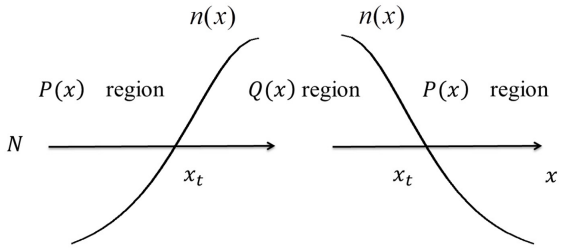

FIG. 1. Index profile $n(x)$ with turning point x_t.

Let us at this point define the following auxiliary functions for subsequent discussions.

$$\eta(x)=\left[\frac{3}{2}\int_x^{x_t}P(x)dx\right]^{2/3} \qquad \xi(x)=\left[\frac{3}{2}\int_{x_t}^{x}Q(x)dx\right]^{2/3} \tag{3a}$$

where

$$P(x)=\sqrt{-\Gamma(x)} \qquad Q(x)=\sqrt{\Gamma(x)} \tag{3b}$$

The MAF trial solutions to (1) are given by a combination of the modified Airy functions as follows:

$$\psi(x)=\begin{cases}\dfrac{c_1}{\sqrt{\xi'(x)}}Ai[-\xi(x)]+\dfrac{c_2}{\sqrt{\xi'(x)}}Bi[-\xi(x)] & \Gamma(x)>0 \quad (4a)\\ \dfrac{c_3}{\sqrt{-\eta'(x)}}Ai[\eta(x)]+\dfrac{c_4}{\sqrt{-\eta'(x)}}Bi[\eta(x)] & \Gamma(x)<0 \quad (4b)\end{cases}$$

where $Ai[-\xi(x)]$ and $Bi[-\xi(x)]$ are Airy functions of the first and second kind, respectively. Asymptotic expressions for these functions are shown in Appendix A and will be used in relating the MAF connection formula to the WKB connection formula.

Note that $Ai(-\xi)$ and $Ai(\eta)$ are continuous at the turning point x_t, as are $Bi(-\xi)$ and $Bi(\eta)$. Thus the boundary condition at each turning point is automatically satisfied under the present MAF trial solution construction.

$$\frac{1}{\sqrt{\xi'(x)}}Ai[-\xi(x)] \quad \leftrightarrow \quad \frac{1}{\sqrt{-\eta'(x)}}Ai[\eta(x)] \tag{5a}$$

$$\frac{1}{\sqrt{\xi'(x)}}Bi[-\xi(x)] \quad \leftrightarrow \quad \frac{1}{\sqrt{-\eta'(x)}}Bi[\eta(x)] \tag{5b}$$

The connection feature of the trial solutions presented in (4) can be seen more clearly through the behavior of a typical wave function, shown in Fig. 2 below.

The MAF trial solutions of (4) take on the following asymptotic forms away from the turning point x_t (see Appendix A).

$$\frac{1}{\sqrt{\xi'(x)}}Ai[-\xi(x)] \approx \frac{1}{\sqrt{\pi Q(x)}}\sin\left(\int_{x_t}^{x}Q(x)dx+\frac{\pi}{4}\right) \tag{6a}$$

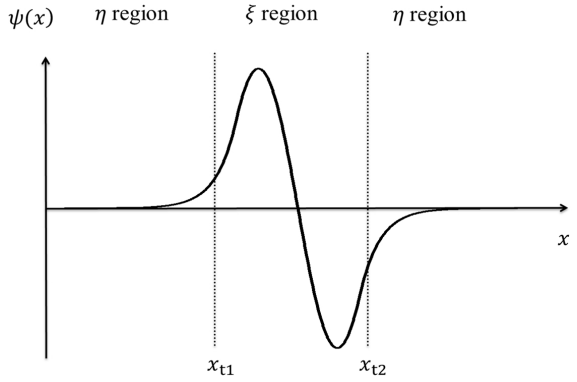

FIG. 2. Connection of MAFs at the turning points x_{t1} and x_{t2}.

$$\frac{1}{\sqrt{-\eta^{'}(x)}}Ai[\eta(x)] \approx \frac{1}{2\sqrt{\pi P(x)}}\exp\left(\int_{x_1}^{x}P(x)dx\right) \quad (6b)$$

$$\frac{1}{\sqrt{\xi^{'}(x)}}Bi[-\xi(x)] \approx \frac{1}{\sqrt{\pi Q(x)}}\cos\left(\int_{x_t}^{x}Q(x)dx+\frac{\pi}{4}\right) \quad (7a)$$

$$\frac{1}{\sqrt{-\eta^{'}(x)}}Bi[\eta(x)] \approx \frac{1}{\sqrt{\pi P(x)}}\exp\left(\int_{x_t}^{x}P(x)dx\right) \quad (7b)$$

The expressions on the right-hand side of (6) and (7) constitute the well-known WKB connection formula, by which (6a) and (7a) are correspondingly transformed into (6b) and (7b), respectively.

III. APPLICATIONS OF THE MAF METHOD TO OPTICAL WAVEGUIDES

3.1. Graded-Index Waveguides

3.1.1. Derivation of Eigenvalue Equation

Consider a planar waveguide with an arbitrary graded-index profile, as shown in Fig. 3.

The one-dimensional Helmholtz equation is

$$\frac{d^2E(x)}{dx^2}+k_0^{\,2}\left(n^2(x)-N^2\right)E(x)=0, \quad (8)$$

where the mode index N and the corresponding field distribution $E(x)$ are the quantities to be solved for. Trial solutions for the planar waveguide of Fig. 3 may be expressed by a combination of the modified Airy functions and the WKB trial solutions depending on the region, as follows [7].

$$E_I(x)=\begin{cases}\dfrac{c_1}{2\sqrt{\pi P(x)}}\exp(-\int_x^a P(x)dx) & x\le a \quad (9a)\\ \dfrac{c_2}{\sqrt{-\eta_1^{'}(x)}}Ai[\eta_1(x)]+\dfrac{c_3}{\sqrt{-\eta_1^{'}(x)}}Bi[\eta_1(x)] & a\le x\le x_{t1} \quad (9b)\end{cases}$$

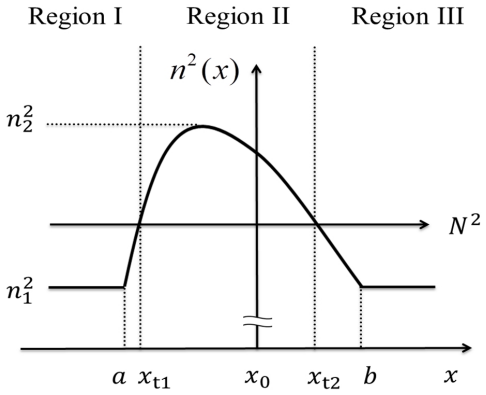

FIG. 3. Graded-index profile $n^2(x)$. x_0 is an arbitrary point between x_{t1} and x_{t2}.

$$E_{II}(x)=\begin{cases}\dfrac{c_2}{\sqrt{\xi_1^{'}(x)}}Ai[-\xi_1(x)]+\dfrac{c_3}{\sqrt{\xi_1^{'}(x)}}Bi[-\xi_1(x)] & x_{t1}\le x\le x_0 \quad (10a)\\ \dfrac{c_4}{\sqrt{-\xi_2^{'}(x)}}Ai[-\xi_2(x)]+\dfrac{c_5}{\sqrt{-\xi_2^{'}(x)}}Bi[-\xi_2(x)] & x_0\le x\le x_{t2} \quad (10b)\end{cases}$$

$$E_{II}(x)=\begin{cases}\dfrac{c_2}{\sqrt{\xi_1^{'}(x)}}Ai[-\xi_1(x)]+\dfrac{c_3}{\sqrt{\xi_1^{'}(x)}}Bi[-\xi_1(x)] & x_{t2}\le x\le b \quad (11a)\\ \dfrac{c_4}{\sqrt{-\xi_2^{'}(x)}}Ai[-\xi_2(x)]+\dfrac{c_5}{\sqrt{-\xi_2^{'}(x)}}Bi[-\xi_2(x)] & b\le x \quad (11b)\end{cases}$$

where

$$\eta_1(x)=\left[\frac{3}{2}\int_x^{x_{t1}}P(x)dx\right]^{2/3} \qquad \xi_1(x)=\left[\frac{3}{2}\int_{x_{t1}}^{x}Q(x)dx\right]^{2/3} \quad (12a)$$

$$\eta_2(x)=\left[\frac{3}{2}\int_{x_{t2}}^{x}P(x)dx\right]^{2/3} \qquad \xi_2(x)=\left[\frac{3}{2}\int_{x}^{x_{t2}}Q(x)dx\right]^{2/3} \quad (12b)$$

$$P(x)=k_0\sqrt{N^2-n^2(x)} \qquad Q(x)=k_0\sqrt{n^2(x)-N^2} \quad (12c)$$

Away from both turning points, the expressions in (10) can be replaced by a linear combination of the sinusoidal functions of (6) and (7), as shown below.

$$E_{II}(x)=\begin{cases}\dfrac{1}{\sqrt{\pi Q(x)}}\left[c_2\sin(\int_{x_{t1}}^{x}Q(x)dx+\frac{\pi}{4})+c_3\cos(\int_{x_{t1}}^{x}Q(x)dx+\frac{\pi}{4})\right] & x_{t1}\le x\le x_0 \quad (13a)\\ \dfrac{1}{\sqrt{\pi Q(x)}}\left[c_4\sin(\int_{x}^{x_{t2}}Q(x)dx+\frac{\pi}{4})+c_5\cos(\int_{x}^{x_{t2}}Q(x)dx+\frac{\pi}{4})\right] & x_0\le x\le x_{t2} \quad (13b)\end{cases}$$

One way to obtain the eigenvalue equation is simply to equate (13a) and (13b). Simple algebraic manipulations lead to the following result.

$$\begin{bmatrix}c_2\\ c_3\end{bmatrix}=\begin{bmatrix}\sin A & \cos A\\ \cos A & -\sin A\end{bmatrix}\begin{bmatrix}c_4\\ c_5\end{bmatrix} \text{ where } A=\int_{x_{t1}}^{x_{t2}}Q(x)dx \quad (14)$$

Another way is to impose boundary conditions requiring that the field and its derivative be continuous at $x=x_0$.

Both approaches lead to the same eigenvalue equation.

$$\int_{x_{t1}}^{x_{t2}} \mathrm{Q}(x)dx = m\pi + \left(\frac{\pi}{4}+\delta_1\right)+\left(\frac{\pi}{4}+\delta_2\right) \tag{15}$$

In the expression above, δ_1 and δ_2 correspond to the phase shifts at the turning points x_{t1} and x_{t2} respectively, and are related to the amplitude coefficients by

$$\delta_1 = \tan^{-1}\left(-c_3/c_2\right) \qquad \delta_2 = \tan^{-1}\left(-c_5/c_4\right) \tag{16}$$

Expressions for δ_1 and δ_2 can be derived by matching the fields and their derivatives at both sides of $x = a$ and $x = b$ respectively, and can be cast in the following forms:

$$\delta_1 = \tan^{-1}\left(\frac{-\eta_1'(a^+)Ai'[\eta_1(a^+)]+P_a Ai[\eta_1(a^+)]}{-\eta_1'(a^+)Bi'[\eta_1(a^+)]+P_a Bi[\eta_1(a^+)]}\right) \tag{17a}$$

$$\delta_2 = \tan^{-1}\left(\frac{\eta_2'(b^-)Ai'[\eta_2(b^-)]+P_b Ai[\eta_2(b^-)]}{\eta_2'(b^-)Bi'[\eta_2(b^-)]+P_b Bi[\eta_2(b^-)]}\right) \tag{17b}$$

where

$$P_a = P(a^-)-\frac{1}{2}\left\{\frac{P'(a^-)}{P(a^-)}-\frac{\eta_1''(a^+)}{\eta_1'(a^+)}\right\} \tag{18a}$$

$$P_b = P(b^+)+\frac{1}{2}\left\{\frac{P'(b^+)}{P(b^+)}-\frac{\eta_2''(b^-)}{\eta_2'(b^-)}\right\} \tag{18b}$$

For a symmetric profile, $\delta_1 = \delta_2$ as expected.

3.1.2. Simulation

To validate the eigenvalue equation of (15), the following parabolic index profile (shown in the inset of Fig. 4) will be assumed.

$$n^2(x) = \begin{cases} n_1^2 & x \le -d \\ n_1^2 + (n_2^2 - n_1^2)\left(1-(x/d)^2\right) & -d \le x \le d \\ n_1^2 & x \ge d \end{cases} \tag{19}$$

To facilitate computation, the normalized frequency v_w and propagation constant b_w, defined below, are utilized.

$$v_w = k_0 d\sqrt{n_2^2 - n_1^2} \qquad b_w = \frac{N^2 - n_1^2}{n_2^2 - n_1^2} \tag{20}$$

(15) can then be cast in the following form, below which the corresponding WKB eigenvalue equation is also presented, for reference.

$$v_w(1-b_w) = (2m+1)+\frac{4}{\pi}\delta_1 \quad : \text{MAF} \tag{21}$$

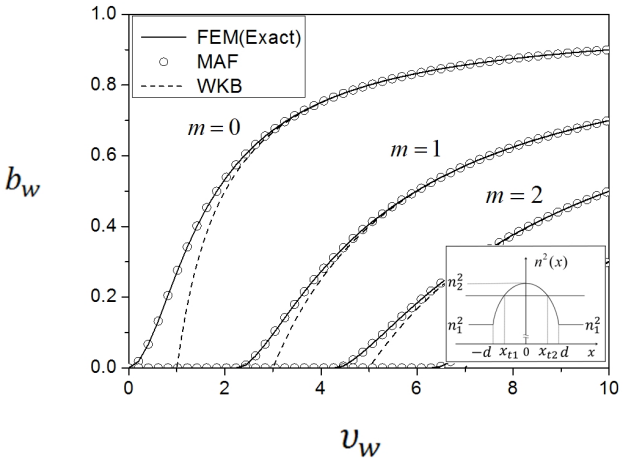

FIG. 4. $v_w - b_w$ curves of a parabolic index profile for the lowest-order modes.

$$v_w(1-b_w) = (2m+1) \quad : \text{WKB} \tag{22}$$

The normalized dispersion curves v_w-b_w for the first several modes are illustrated in Fig. 4, which also includes the exact numerical solution obtained via FEM for comparison. The figure clearly shows excellent agreement between the MAF result and the exact result, thus validating the use of the MAF method, whereas the WKB curves show some deviations near the cutoff points as expected.

3.2. Truncated Graded-Index Waveguides

3.2.1. Derivation of Eigenvalue Equation

Consider a truncated graded-index profile, as shown in the inset of Fig. 5. Notice that the left turning point now coincides with the location of the index discontinuity. MAF trial solutions appropriate for this structure can be written as follows.

$$E_I(x) = \frac{c_1}{2\sqrt{\pi P(x)}}\exp\left(-\int_x^0 P(x)dx\right), \qquad x \le 0 \tag{23}$$

$$E_{II}(x) = \frac{c_2}{\sqrt{-\xi'(x)}}Ai[-\xi(x)]+\frac{c_3}{\sqrt{-\xi'(x)}}Bi[-\xi(x)], \qquad 0 \le x \le x_t \tag{24}$$

$$E_{III}(x) = \begin{cases} \dfrac{c_2}{\sqrt{\eta'(x)}}Ai[\eta(x)]+\dfrac{c_3}{\sqrt{\eta'(x)}}Bi[\eta(x)], & x_t \le x \le d \quad (25a) \\ \dfrac{c_4}{2\sqrt{\pi P(x)}}\exp\left(-\int_d^x P(x)dx\right), & d \le x \quad (25b) \end{cases}$$

where the definitions of $\eta(x)$, $\xi(x)$, and $P(x)$ are identical to those given by the expressions for $\eta_2(x)$, $\xi_2(x)$, and $P(x)$ in (12), respectively, with x_2 now replaced by x_t.

By applying a procedure similar to that of the previous section, the eigenvalue equation can be obtained as follows.

$$\int_0^{x_t} Q(x)dx = m\pi + \frac{\pi}{4} + \tan^{-1}\left(\sqrt{\frac{a_w + b_w}{1 - b_w}}\right) + \delta \tag{26}$$

where

$$b_w = \frac{N^2 - {n_3}^2}{{n_2}^2 - {n_3}^2} \qquad a_w = \frac{{n_3}^2 - {n_1}^2}{{n_2}^2 - {n_3}^2} \tag{27}$$

While the δ term in (26) represents the phase shift at the turning point $x = d$, the inverse-tangent term represents the phase shift at $x = 0$, the point of index discontinuity.

$$\delta = \tan^{-1}\left(\frac{\eta'(d^-)Ai'[\eta(d^-)] + P_d Ai[\eta(d^-)]}{\eta'(d^-)Bi'[\eta(d^-)] + P_d Bi[\eta(d^-)]}\right) \tag{28}$$

where

$$P_d = P(d^+) + \frac{1}{2}\left\{\frac{P'(d^+)}{P(d^+)} - \frac{\eta''(d^-)}{\eta'(d^-)}\right\} \tag{29}$$

3.2.2. Simulation

The truncated parabolic index profile of Fig. 5 is described as

$$n^2(x) = \begin{cases} n_1^2 & x \le 0 \\ n_3^2 + (n_2^2 - n_3^2)\left(1 - (x/d)^2\right) & 0 \le x \le d \\ n_3^2 & x \ge d \end{cases} \tag{30}$$

For this truncated profile, the eigenvalue equation of (26) can be cast in the following form. The WKB eigenvalue equation is also presented, for reference.

$$\upsilon_w(1 - b_w) = (4m+1) + \frac{4}{\pi}\tan^{-1}\left(\sqrt{\frac{a_w + b_w}{1 - b_w}}\right) + \frac{4}{\pi}\delta \quad : \text{MAF} \tag{31}$$

$$\upsilon_w(1 - b_w) = (4m+1) + \frac{4}{\pi}\tan^{-1}\left(\sqrt{\frac{a_w + b_w}{1 - b_w}}\right) \quad : \text{WKB} \tag{32}$$

Calculation results based on the eigenvalue equation of (31) are displayed in Fig. 5 along with the corresponding WKB and FEM results. As was the case for the symmetric parabolic index profile (see Fig. 4), the MAF results show excellent agreement with the exact FEM results, while the WKB curves show minor deviations near the cutoff regions.

Based on this and the previous result, it may be concluded that the MAF technique provides a rather robust and highly accurate method for analysis of a wide range of graded-index optical waveguides.

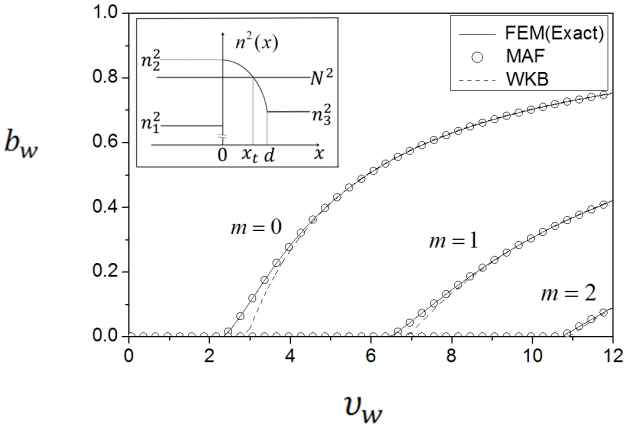

FIG. 5. υ_w-b_w curves of a truncated graded-index profile for the lowest-order modes.

IV. APPLICATIONS OF THE MAF METHOD TO TUNNELING PROBLEMS

The MAF-based approach will now be applied to a set of barrier profiles, to test its feasibility in tunneling analysis. The one-dimensional Schrödinger equation takes the form

$$\frac{d^2\psi(x)}{dx^2} + \frac{2m}{\hbar^2}[E - V(x)]\psi(x) = 0 \tag{33}$$

Hereafter, we will work in atomic units where $m = \hbar = 1$, with x and E in the units of Bohr and Hartree, respectively.

4.1. Graded Potential Barriers

4.1.1. Derivation of Tunneling Probability

Consider a potential barrier as shown in Fig. 6, with particle energy E. Trial solutions similar to those employed in the optical waveguide analysis can also be used in this case [7].

$$\psi_I(x) = \begin{cases} c_1 \exp(\mathrm{j}\int_x^a q_0 dx) + c_2 \exp(-\mathrm{j}\int_x^a q_0 dx) & x \le a \quad (34a) \\ \dfrac{c_3}{\sqrt{-\xi_1'(x)}} Ai(-\xi_1(x)) + \dfrac{c_4}{\sqrt{-\xi_1'(x)}} Bi(-\xi_1(x)) & a \le x \le x_{t1} \quad (34b) \end{cases}$$

$$\psi_{II}(x) = \begin{cases} \dfrac{c_3}{\sqrt{\eta_1'(x)}} Ai(\eta_1(x)) + \dfrac{c_4}{\sqrt{\eta_1'(x)}} Bi(\eta_1(x)) & x_{t1} \le x \le x_p \quad (35a) \\ \dfrac{c_5}{\sqrt{-\eta_2'(x)}} Ai(\eta_2(x)) + \dfrac{c_6}{\sqrt{-\eta_2'(x)}} Bi(\eta_2(x)) & x_p \le x \le x_{t2} \quad (35b) \end{cases}$$

$$\psi_{III}(x) = \begin{cases} \dfrac{c_5}{\sqrt{\xi_2'(x)}} Ai(-\xi_2(x)) + \dfrac{c_6}{\sqrt{\xi_2'(x)}} Bi(-\xi_2(x)) & x_{t2} \le x \le b \quad (36a) \\ c_7 \exp(-\mathrm{j}\int_b^x q_0 dx) & b \le x \quad (36b) \end{cases}$$

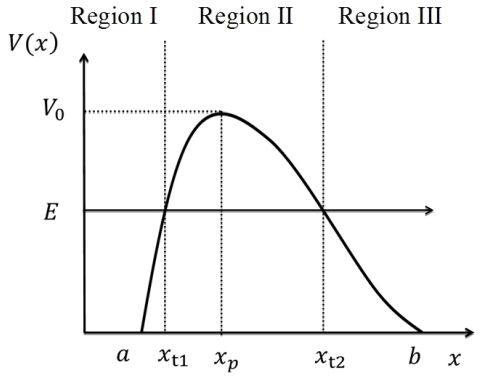

FIG. 6. Graded potential barrier. x_p is the location of the potential peak V_0.

where

$$\eta_1(x)=\left[\frac{3}{2}\int_{x_{t1}}^{x} p(x)dx\right]^{2/3} \qquad \xi_1(x)=\left[\frac{3}{2}\int_{x}^{x_{t1}} q(x)dx\right]^{2/3} \tag{37a}$$

$$\eta_2(x)=\left[\frac{3}{2}\int_{x}^{x_{t2}} p(x)dx\right]^{2/3} \qquad \xi_2(x)=\left[\frac{3}{2}\int_{x_{t2}}^{x} q(x)dx\right]^{2/3} \tag{37b}$$

$$p(x)=\sqrt{2(V(x)-\mathrm{E})} \quad q(x)=\sqrt{2(E-V(x))} \quad q_0=\sqrt{2E} \tag{38}$$

$\eta(x)$ is defined where $V(x)$ is higher than E, and $\xi(x)$ where $V(x)$ is lower than E. Note that trial functions on both sides of each turning point satisfy the boundary condition automatically as before, via 'the MAF connection formula.'

Suppose the expressions of (35) are replaced by the following asymptotic forms (see Appendix A) much like in the earlier waveguide section but with different forms here.

$$\psi_{II}(x)=\begin{cases}\dfrac{c_3}{2\sqrt{\pi p(x)}}\exp\left[-\int_{x_{t1}}^{x} p(x)dx\right]+\dfrac{c_4}{\sqrt{\pi p(x)}}\exp\left[\int_{x_{t1}}^{x} p(x)dx\right] & x_{t1}\le x\le x_p \quad (39a)\\ \dfrac{c_5}{2\sqrt{\pi p(x)}}\exp\left[-\int_{x}^{x_{t2}} p(x)dx\right]+\dfrac{c_6}{\sqrt{\pi p(x)}}\exp\left[\int_{x}^{x_{t2}} p(x)dx\right] & x_p\le x\le x_{t2} \quad (39b)\end{cases}$$

Either by equating these two equations or by imposing the boundary conditions at a point between the two turning points, the following relation may be obtained.

$$\begin{bmatrix}c_3\\ c_4\end{bmatrix}=\begin{bmatrix}0 & 2\exp(A)\\ \frac{1}{2}\exp(-A) & 0\end{bmatrix}\begin{bmatrix}c_5\\ c_6\end{bmatrix} \text{ where } A=\int_{x_{t1}}^{x_{t2}} p(x)dx \tag{40}$$

At this point, it must be noted that the computation results based on (40) were nearly identical to those obtained from the WKB analysis. This is in clear contrast to the case of the optical waveguide, where use of asymptotic forms of the MAF trial solutions led to very accurate results that were distinctly different from the WKB results.

We shall now revert to the trial solutions of (34) to (36) as they are, and impose the boundary conditions at $x=a$, x_p, and b, respectively. Applying the continuity of the field and its derivative at the boundary point $x=a$, we obtain the following matrix relation:

$$\begin{bmatrix}1 & 1\\ -jq_0 & jq_0\end{bmatrix}\begin{bmatrix}c_1\\ c_2\end{bmatrix}=\begin{bmatrix}A_1(\mathrm{a}^+) & B_1(\mathrm{a}^+)\\ A_1'(\mathrm{a}^+) & B_1'(\mathrm{a}^+)\end{bmatrix}\begin{bmatrix}c_3\\ c_4\end{bmatrix} \tag{41}$$

where

$$A_1(a^+)=\frac{1}{\sqrt{-\xi_1'(a^+)}}Ai\left(-\xi_1(a^+)\right) \quad B_1(a^+)=\frac{1}{\sqrt{-\xi_1'(a^+)}}Bi\left(-\xi_1(a^+)\right) \tag{42}$$

Next, boundary condition matching at $x=x_p$ yields

$$\begin{bmatrix}A_2(x_p) & B_2(x_p)\\ A_2'(x_p) & B_2'(x_p)\end{bmatrix}\begin{bmatrix}c_3\\ c_4\end{bmatrix}=\begin{bmatrix}A_3(x_p) & B_3(x_p)\\ A_3'(x_p) & B_3'(x_p)\end{bmatrix}\begin{bmatrix}c_5\\ c_6\end{bmatrix} \tag{43}$$

where

$$A_2(x_p)=\frac{1}{\sqrt{\eta_1'(x_p)}}Ai\left(\eta_1(x_p)\right) \quad B_2(x_p)=\frac{1}{\sqrt{\eta_1'(x_p)}}Bi\left(\eta_1(x_p)\right) \tag{44a}$$

$$A_3(x_p)=\frac{1}{\sqrt{-\eta_2'(x_p)}}Ai\left(\eta_2(x_p)\right) \quad B_3(x_p)=\frac{1}{\sqrt{-\eta_2'(x_p)}}Bi\left(\eta_2(x_p)\right) \tag{44b}$$

Finally, application of the boundary conditions at $x=b$ yields the following relation:

$$\begin{bmatrix}A_4(b^-) & B_4(b^-)\\ A_4'(b^-) & B_4'(b^-)\end{bmatrix}\begin{bmatrix}c_5\\ c_6\end{bmatrix}=\begin{bmatrix}1\\ -jq_0\end{bmatrix}c_7 \tag{45}$$

where

$$A_4(b^-)=\frac{1}{\sqrt{\xi_2'(b^-)}}Ai\left(-\xi_2(b^-)\right) \; B_4(b^-)=\frac{1}{\sqrt{\xi_2'(b^-)}}Bi\left(-\xi_2(b^-)\right) \tag{46}$$

Equations (41), (43), and (45) can be combined to yield the following overall matrix equation relating c_1, c_2 and c_7.

$$\begin{bmatrix}c_1\\ c_2\end{bmatrix}=\begin{bmatrix}1 & 1\\ -jq_0 & jq_0\end{bmatrix}^{-1}\begin{bmatrix}A_1 & B_1\\ A_1' & B_1'\end{bmatrix}\begin{bmatrix}A_2 & B_2\\ A_2' & B_2'\end{bmatrix}^{-1}\begin{bmatrix}A_3 & B_3\\ A_3' & B_3'\end{bmatrix}\begin{bmatrix}A_4 & B_4\\ A_4' & B_4'\end{bmatrix}^{-1}\begin{bmatrix}1\\ -jq_0\end{bmatrix}c_7 \tag{47}$$

It follows from (47) that the tunneling probability is given by the expression below.

$$T_{MAF}=\left|\frac{c_7}{c_1}\right|^2=\left|\frac{j2q_0\Delta_1\Delta_2}{A_1^*B_T+A_TB_1^*}\right|^2 \tag{48}$$

Detailed descriptions of the terms Δ_1, Δ_2, A_1^*, B_1^*, A_T, and B_T are available in [9].

Derivation of the tunneling probability using the WKB method for a graded potential barrier is presented in Appendix B-1.

4.1.2. Simulation

Case 1: Symmetric exponential potential barrier

To verify the validity of the MAF formulation for graded potential barriers, a symmetric exponential profile (shown in the inset of Fig. 7) was selected as the first test case. The calculated results based on (48) are displayed in the figure, along with the results obtained by the exact transfer matrix (TM) method. The WKB results are also included, for reference.

Figure 7 clearly shows that the MAF method leads to solutions with very high accuracy over the entire region of E/V_0. Meanwhile, the WKB method is seen to produce results with noticeable deviations, which is expected, given the WKB method's inherent deficiencies.

Case 2: Parabolic potential barrier

A parabolic potential barrier is taken as the second example, and is shown in the inset of Fig. 8.

Calculated results for this profile are illustrated in Fig. 8. The WKB results show behavior similar to that in Fig. 7. However, the MAF results show tunneling probabilities much lower than the true values across the entire range, contrary to expectation; part of this tendency can in fact be observed in the previous reports of [6, 11] upon careful examination. Even more disturbing, the calculation results fall to zero as E/V_0 approaches unity; the causes of this phenomenon are as follows. According to our investigation described in Appendix C, when E approaches V_0, the denominators of the terms in (35) containing $\eta'(x_p)$ go to zero, causing the

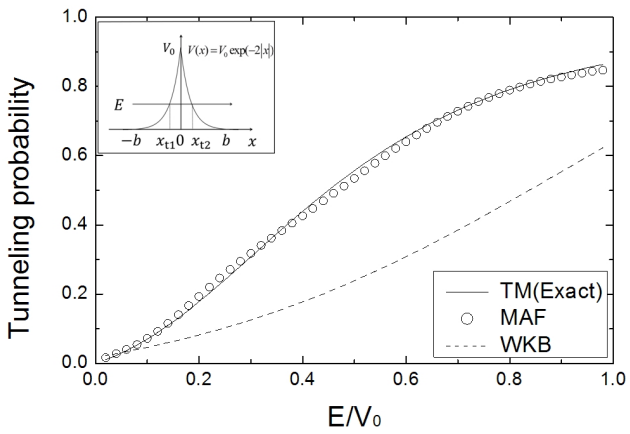

FIG. 7. Tunneling probabilities for a symmetric exponential barrier with $x_p = 0$, $V_0 = 1$, and $b = 5$.

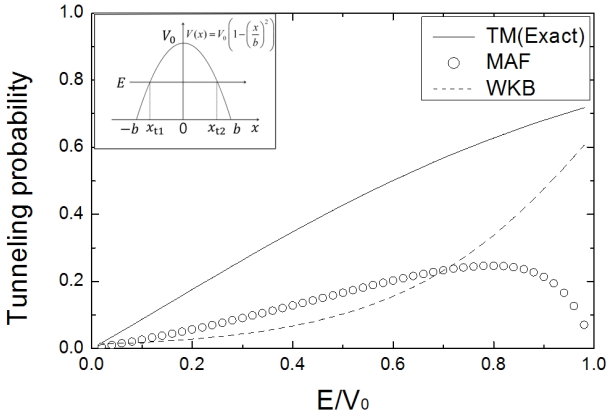

FIG. 8. Tunneling probabilities for a parabolic barrier with $x_p = 0$, $V_0 = 1$, and $b = 1$.

trial functions to become singular. As the trial functions in (34a) representing the incident and reflected components are finite, the coefficients of the trial functions in region II must go to zero, to satisfy the boundary conditions at $x = -b$. This in turn leads the coefficient in the transmitted region, and thus the tunneling probability, to vanish. It turns out that whenever $V'(x_p) = 0$, $\eta'(x_p)$ vanishes in the limit of $E \to V_0$, leading to the failure of the MAF method.

4.2. Truncated Potential Barriers

4.2.1. Derivation of Tunneling Probability

Consider a truncated graded potential barrier, as shown in Fig. 9.

For the truncated graded barrier in Fig. 9, the trial solutions may be taken to be

$$\psi_I(x) = c_1 \exp(\mathrm{j}\int_x^a q_0 dx) + c_2 \exp(-\mathrm{j}\int_x^a q_0 dx) \qquad x \le a \qquad (49)$$

$$\psi_{II}(x) = \frac{c_3}{\sqrt{-\eta'(x)}} Ai(\eta(x)) + \frac{c_4}{\sqrt{-\eta'(x)}} Bi(\eta(x)) \qquad a \le x \le x_t \qquad (50)$$

$$\psi_{III}(x) = \begin{cases} \dfrac{c_3}{\sqrt{\xi'(x)}} Ai(-\xi(x)) + \dfrac{c_4}{\sqrt{\xi'(x)}} Bi(-\xi(x)) & x_t \le x \le b \quad (51a) \\ c_5 \exp(-\mathrm{j}\int_b^x q_0 dx) & b \le x \quad (51b) \end{cases}$$

where

$$\eta(x) = \left[\frac{3}{2}\int_x^{x_t} p(x)dx\right]^{2/3} \quad \xi(x) = \left[\frac{3}{2}\int_{x_t}^{x} q(x)dx\right]^{2/3} \qquad (52)$$

By applying the boundary conditions at $x = a$, x_t, and b and manipulating the resulting equations, the following matrix equation can be obtained.

$$\begin{bmatrix} c_1 \\ c_2 \end{bmatrix} = \begin{bmatrix} 1 & 1 \\ -jq_0 & jq_0 \end{bmatrix}^{-1} \begin{bmatrix} A_1 & B_1 \\ A_1' & B_1' \end{bmatrix} \begin{bmatrix} A_2 & B_2 \\ A_2' & B_2' \end{bmatrix}^{-1} \begin{bmatrix} 1 \\ -jq_0 \end{bmatrix} c_5 \qquad (53)$$

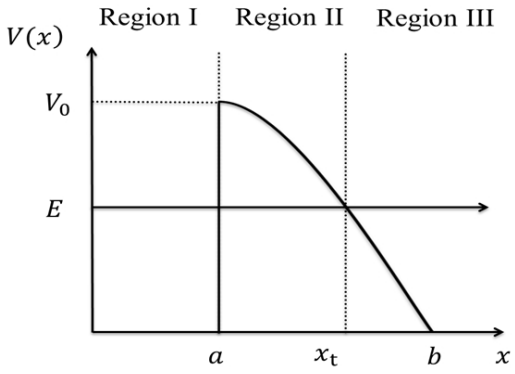

FIG. 9. Truncated graded potential barrier.

It follows that the tunneling probability is then given by

$$T_{MAF} = \left|\frac{c_5}{c_1}\right|^2 = \left|\frac{j2q_0\Delta}{A_1^* B_2^* + A_2^* B_1^*}\right|^2 \tag{54}$$

Detailed descriptions of the terms Δ, A_1^*, B_1^*, A_2^*, and B_2^* are available in [9]. Meanwhile, the tunneling probability for truncated potential barriers based on the WKB method has also been derived in Appendix B-2.

4.2.2. Simulation

Here the same two potential profiles analyzed in the previous section shall be examined, but with the left half of each profile removed.

Case 1: Truncated exponential potential barrier

Let us take the truncated exponential potential barrier of the inset of Fig. 10 as the first example.

The calculated results based on (54) are displayed in Fig. 10, which shows excellent agreement between the MAF results and the exact TM results. It is seen that the WKB results, on the other hand, fail: As E/V_0 approaches unity, the tunneling probability falls to zero. The causes of this behavior can be stated as follows. At $x = 0$, the truncation point, the denominators of the terms in (B8) for the region II go to zero as E approaches V_0, thereby driving the trial functions to become divergent. It then follows that the coefficients of the trial functions in the region II must go to zero, for the same reason mentioned in the previous case of Fig. 8. This in turn leads to the coefficients of the trial function in the transmitted region, and thus the tunneling probability, to vanish. Based on this finding it may be concluded that whenever there is a truncation in the barrier, the denominator of the trial functions vanishes in the limit of $E \to V_0$, leading to the failure of the WKB method.

Case 2: Truncated parabolic potential barrier

A truncated parabolic potential barrier, shown in the inset of Fig. 11, is taken as the second example.

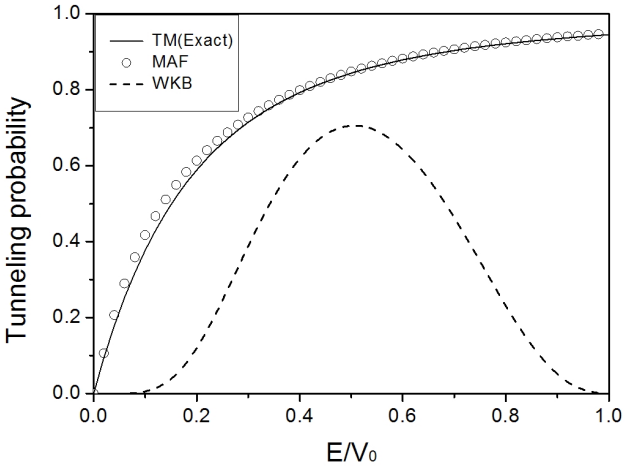

FIG. 10. Tunneling probabilities for a truncated exponential barrier with V_0=1 and b=5.

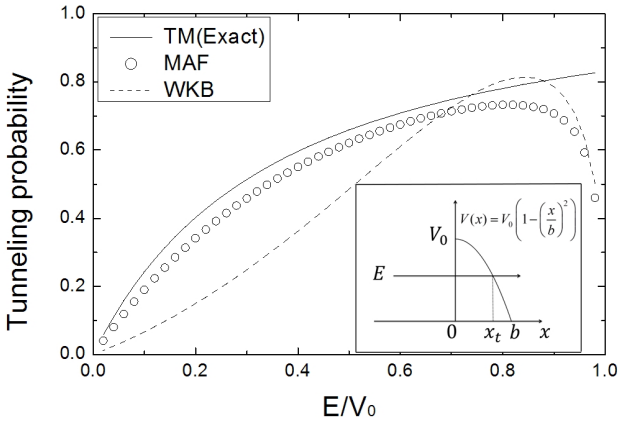

FIG. 11. Tunneling probabilities for a truncated parabolic barrier with V_0=1 and b=1.

Simulation results are illustrated in Fig. 11. The results are interesting in that both the MAF and the WKB curves deviate significantly from the exact solution, and fall to 0 as E/V_0 approaches unity. The reasons for the failure of each respective result are as stated previously: the presence of $V'(x_p) = 0$ in the case of the MAF application, and the very presence of a truncation in the case of the WKB application. Such characteristics of potential barriers can be traced to the divergence of the associated trial solutions in region II in the limit of $E \to V_0$, which finally causes the tunneling probability to fall to zero. That the MAF result fares much better (except for E/V_0 in the range of unity) compared to the symmetric parabolic case of Fig. 8 can be attributed to the fact that the barrier width has been reduced by a factor of one half, thereby increasing the transmission probability, and that the barrier shape has been altered, leading to mitigation of the trial solution's failure associated with a smooth peak.

V. CONCLUSION

The plausibility of applying the MAF method to the analysis of graded optical waveguides and potential barriers was reviewed in this paper, with the conventional WKB method serving as a basis for comparison. Application of the MAF technique to the waveguide problem led to satisfactory results for both symmetric and truncated graded-index distributions, in that it was possible to derive a simple closed-form eigenvalue equation, and the calculated results were very accurate. When the same MAF approach was applied to the problem of tunneling probability in the presence of a graded potential barrier, however, the results were mixed, which was contrary to our initial expectation. The MAF method turns out to be inadequate in any case with $V'(x_p) = 0$, that is, when the potential contains a smooth peak, causing the trial functions to diverge at the peak location x_p in the $E \rightarrow V_0$ limit. The WKB approach fails as well for profiles with truncation, because of the diverging trial functions at the truncation point in the same limit.

The discrepancy between the end results from the MAF analysis for the two classes of problems, graded-index optical waveguide and graded potential barrier, is believed to stem from the different respective natures of the two problems. In the waveguide problem only discrete eigenvalues are allowed, and any mode index N obtained must be less than the peak value of the given index profile, thereby avoiding in the first place the problem of divergence of the trial solutions. In the tunneling problem, however, the concept of discrete eigenvalues does not apply; E the particle energy E is continuous-valued and can be chosen arbitrarily, including the $E \rightarrow V_0$ case, which can cause the trial solutions to become singular. The same reason remains valid with the WKB method.

It may thus be concluded that the MAF method is not appropriate for analysis of tunneling problems in which graded potential barriers with the condition of $V'(x_p) = 0$ are involved. It also may be added that the WKB method is not suitable for tunneling problems involving abruptly truncated barriers.

APPENDIX A. CONNECTION FORMULAE OF MAF SOLUTIONS

Asymptotic forms of the Airy functions are [13]

$$Ai(z) \approx \frac{1}{\sqrt{\pi}(-z)^{1/4}} \sin\left[\frac{2}{3}(-z)^{3/2} + \frac{\pi}{4}\right] \qquad z << 0 \quad \text{(A1)}$$

$$Ai(z) \approx \frac{1}{2\sqrt{\pi}(z)^{1/4}} \exp\left[-\frac{2}{3}z^{3/2}\right] \qquad z >> 0 \quad \text{(A2)}$$

$$Bi(z) \approx \frac{1}{\sqrt{\pi}(-z)^{1/4}} \cos\left[\frac{2}{3}(-z)^{3/2} + \frac{\pi}{4}\right] \qquad z << 0 \quad \text{(A3)}$$

$$Bi(z) \approx \frac{1}{\sqrt{\pi}(z)^{1/4}} \exp\left[\frac{2}{3}z^{3/2}\right] \qquad z >> 0 \quad \text{(A4)}$$

The MAF trial solutions in Section II can be converted to the well-known WKB solutions with the aid of the above asymptotic approximations.

$$\frac{1}{\sqrt{\xi'(x)}} Ai(-\xi(x)) \approx \frac{1}{\sqrt{\pi}(\xi)^{1/4}} \frac{1}{\sqrt{\xi'(x)}} \sin\left[\frac{2}{3}(\xi)^{3/2} + \frac{\pi}{4}\right] = \frac{1}{\sqrt{\pi Q(x)}} \sin\left[\int_{x_t}^{x} Q(x)dx + \frac{\pi}{4}\right] \quad \text{(A5)}$$

$$\frac{1}{\sqrt{\xi'(x)}} Bi[-\xi(x)] \approx \frac{1}{\sqrt{\pi}(\xi)^{1/4}} \frac{1}{\sqrt{\xi'(x)}} \cos\left[\frac{2}{3}(\xi)^{3/2} + \frac{\pi}{4}\right] = \frac{1}{\sqrt{\pi Q(x)}} \cos\left[\int_{x_t}^{x} Q(x)dx + \frac{\pi}{4}\right] \quad \text{(A6)}$$

$$\frac{1}{\sqrt{-\eta'(x)}} Ai[\eta(x)] \approx \frac{1}{2\sqrt{\pi}(\eta(x))^{1/4}} \frac{1}{\sqrt{-\eta'(x)}} \exp\left[-\frac{2}{3}\eta(x)^{3/2}\right] = \frac{1}{2\sqrt{\pi P(x)}} \exp\left[-\int_{x_t}^{x} P(x)dx\right] \quad \text{(A7)}$$

$$\frac{1}{\sqrt{-\eta'(x)}} Bi[\eta(x)] \approx \frac{1}{\sqrt{\pi}(\eta(x))^{1/4}} \frac{1}{\sqrt{-\eta'(x)}} \exp\left[\frac{2}{3}\eta(x)^{3/2}\right] = \frac{1}{\sqrt{\pi P(x)}} \exp\left[\int_{x_t}^{x} P(x)dx\right] \quad \text{(A8)}$$

where

$$\eta(x) = \left[\frac{3}{2}\int_{x}^{x_t} P(x)dx\right]^{2/3} \qquad \xi(x) = \left[\frac{3}{2}\int_{x_t}^{x} Q(x)dx\right]^{2/3} \quad \text{(A9)}$$

Note that the equations in the right-most column in (A5)-(A8) are the well-known WKB functions.

APPENDIX B. WKB ANALYSIS

B-1. Tunneling Probability for a Graded Potential Barrier

The WKB solutions can be expressed as follows for the problem of tunneling through the graded potential barrier depicted in Fig. 6:

$$\psi_I(x) = \frac{c_1}{\sqrt{q(x)}} \exp\left(\mathrm{j}\int_{x}^{x_{t1}} q(x)dx\right) + \frac{c_2}{\sqrt{q(x)}} \exp\left(-\mathrm{j}\int_{x}^{x_{t1}} q(x)dx\right) \qquad x \le x_{t1} \quad \text{(B1)}$$

$$\psi_{II}^{<}(x) = \frac{c_3}{\sqrt{p(x)}} \exp\left(\int_{x_{t1}}^{x} p(x)dx\right) + \frac{c_4}{\sqrt{p(x)}} \exp\left(-\int_{x_{t1}}^{x} p(x)dx\right) \quad x_{t1} \le x \le x_{t2} \quad \text{(B2)}$$

$$\psi_{II}^{>}(x) = \frac{c_5}{\sqrt{p(x)}} \exp\left(\int_{x}^{x_{t2}} p(x)dx\right) + \frac{c_6}{\sqrt{p(x)}} \exp\left(-\int_{x}^{x_{t2}} p(x)dx\right) \quad x_{t1} \le x \le x_{t2} \quad \text{(B3)}$$

$$\psi_{III}(x) = \frac{c_7}{\sqrt{q(x)}} \exp\left(-\mathrm{j}\int_{x_{t2}}^{x} q(x)dx\right) \qquad x \ge x_{t2} \quad \text{(B4)}$$

where

$$p(x) = \sqrt{2(V(x) - E)} \qquad q(x) = \sqrt{2(E - V(x))} \quad \text{(B5)}$$

Boundary condition matching at x_{t1} and x_{t2} leads to

$$T_{WKB} = \left(D + 1/(4D)\right)^{-2} \quad \text{where} \quad D = \exp\left(\int_{x_{t1}}^{x_{t2}} p(x)dx\right) \quad \text{(B6)}$$

B-2. Tunneling Across a Truncated Graded Potential Barrier

For the case of tunneling through a truncated potential barrier with graded profile shown in Fig. 9, the trial solution

in each constituent region can be expressed in the following manner:

$$\psi_I(x) = c_1 \exp\left(\mathrm{j}\int_x^a q_0 dx\right) + c_2 \exp\left(-\mathrm{j}\int_x^a q_0 dx\right) \qquad x \le a \quad \text{(B7)}$$

$$\psi_{II}(x) = \frac{c_3}{\sqrt{p(x)}} \exp\left(\int_x^{x_t} p(x)dx\right) + \frac{c_4}{\sqrt{p(x)}} \exp\left(-\int_x^{x_t} p(x)dx\right) \qquad a \le x \le x_t \quad \text{(B8)}$$

$$\psi_{III}(x) = \frac{c_5}{\sqrt{q(x)}} \exp\left(-\mathrm{j}\int_{x_t}^{x} q(x)dx\right) \qquad x \le x_t \quad \text{(B9)}$$

where

$$p(x) = \sqrt{2(V(x)-E)} \qquad q(x) = \sqrt{2(E-V(x))} \qquad q_0 = \sqrt{2E} \quad \text{(B10)}$$

Applying the boundary conditions at $x = a$ and using the connection formula at $x = x_t$, the following expression can be obtained for the tunneling probability.

$$T_{WKB} = \left| \frac{2}{K_1 D - \frac{j}{2}\frac{K_2}{D}} \right|^2 \qquad \text{where} \quad D = \exp\left(\int_a^{x_t} p(x)dx\right) \quad \text{(B11)}$$

where

$$K_{1,2} = \left[\frac{1}{\sqrt{p(a)}} + \frac{j}{q_0} \left\{ \frac{d}{dx}\left(\frac{1}{\sqrt{p(x)}} \right)\bigg|_{x=a} \mp \sqrt{p(a)} \right\} \right] \quad \text{(B12)}$$

with the subscripts 1 and 2 corresponding to '-' and '+' signs respectively.

APPENDIX C. LIMITING BEHAVIORS OF $\eta'(x)$

The MAF trial solutions introduced earlier contain the factor $\sqrt{\eta'(x)}$ in the denominator. Here it will be proven that $\eta'(x)$ becomes zero in certain limiting cases, causing the trial functions to become singular, and leading to the failure of the MAF analysis in the end. Two limiting cases will be explored:

(1) What happens to $\eta'(x)$ at the turning point x_t?
(2) What happens to $\eta'(x)$ at $x = x_p$ as E approaches V_0 (x_p being the location of the potential peak)?

As before, we start with

$$\eta(x) = \left[\frac{3}{2}\int_x^{x_t} p(x)dx \right]^{2/3} \quad \text{(C1)}$$

$$p(x) = \sqrt{2(V(x)-E)} \quad \text{(C2)}$$

C-1. Limiting Behavior of $\eta'(x)$ at the Turning Point x_t

From (C1), it follows that

$$\eta'(x) = \frac{-p(x)}{\left[\frac{3}{2}\int_x^{x_t} p(x)dx \right]^{1/3}} \quad \text{(C3)}$$

We begin by rewriting (C3) and taking the limit $x \to x_t$.

$$\lim_{x\to x_t} \eta'(x) = \lim_{x\to x_t} \left[\frac{-p^3(x)}{\frac{3}{2}\int_x^{x_t} p(x)dx} \right]^{1/3} \quad \text{(C4)}$$

Applying L'Hopital's rule by differentiating both numerator and the denominator with respect to x, we obtain

$$\lim_{x\to x_t} \eta'(x) = \lim_{x\to x_t} \left[\frac{-3V'(x)p(x)}{-\frac{3}{2}p(x)} \right]^{1/3} = \left[2V'(x_t) \right]^{1/3} \quad \text{(C5)}$$

Thus the limiting behavior of $\eta'(x)$ is directly related to the slope of the potential barrier at x_t. As such, so long as the slope of the potential is not zero at the turning point, which is usually the case, the MAF trial solution is not divergent.

C-2. Limiting Behavior of $\eta'(x)$ at $x = x_p$ as $E \to V_0$

To facilitate further discussion, (C3) and (C2) will be respectively expressed as follows.

$$\eta'(x_p; x_t) = \frac{-p(x_p; x_t)}{\left[\frac{3}{2}\int_{x_p}^{x_t} p(x; x_t)dx \right]^{1/3}} \quad \text{(C6)}$$

$$p(x; x_t) = \sqrt{2(V(x)-E)} = \sqrt{2(V(x)-V(x_t))} \quad \text{(C7)}$$

from which it follows that

$$p'(x; x_t) = \frac{\partial p(x; x_t)}{\partial x} = \frac{V'(x)}{\sqrt{2(V(x)-V(x_t))}} = \frac{V'(x)}{p(x; x_t)} \quad \text{(C8)}$$

$$\frac{\partial p(x; x_t)}{\partial x_t} = \frac{-\frac{dV(x_t)}{dx_t}}{\sqrt{2(V(x)-V(x_t))}} = \frac{-\frac{dV(x_t)}{dx_t}}{p(x; x_t)} \quad \text{(C9)}$$

Clearly the numerator and denominator of the expression in (C6) both go to zero in the limit $x_t \to x_p$ ($E \to V_0$). By taking the limit

$$\lim_{x_t\to x_p} \eta'(x_p; x_t) = \lim_{x_t\to x_p} \left[\frac{-p^3(x_p; x_t)}{\frac{3}{2}\int_{x_p}^{x_t} p(x; x_t)dx} \right]^{1/3} \quad \text{(C10)}$$

and applying L'Hopital's rule once again, this time along with Leibniz's rule of integration, we obtain

$$\lim_{x_t \to x_p} \eta'(x_p; x_t) = \lim_{x_t \to x_p} \left[\frac{3 \dfrac{dV(x_t)}{dx_t} p(x_p; x_t)}{\dfrac{3}{2} \displaystyle\int_{x_p}^{x_t} \frac{\partial p(x; x_t)}{\partial x_t} dx} \right]^{1/3} \tag{C11}$$

The expression above can further be simplified by applying (C9) to the denominator as well:

$$\lim_{x_t \to x_p} \eta'(x_p; x_t) = \lim_{x_t \to x_p} \left[\frac{-2}{\displaystyle\int_{x_p}^{x_t} \frac{1}{p(x; x_t) p(x_p; x_t)} dx} \right]^{1/3} \tag{C12}$$

Suppose the potential distribution in the vicinity of the peak location x_p is represented by a linear approximation:

$$V(x) \approx V_0 \left[1 - b(x - x_p) \right] \tag{C13}$$

The integral in the denominator of (C12) now reduces to

$$\frac{1}{2V_0 b \sqrt{x_t - x_p}} \int_{x_p}^{x_t} \frac{dx}{\sqrt{x_t - x}} = \frac{1}{V_0 b} \tag{C14}$$

Substituting this result into (C12) and recognizing that $V_0 b$ in (C14) is the negative of the potential's slope, we have

$$\lim_{x_t \to x_p} \eta'(x_p; x_t) = \left[-2 V_0 b \right]^{1/3} = \left[2 V'(x_p) \right]^{1/3} \tag{C15}$$

Thus we have shown that $\eta'(x)$ approaches $[2V'(x_p)]^{1/3}$ in the limit of $E \to V_0$. If the slope of the potential barrier is nonzero at the peak, then $\eta'(x_t)$ is nonzero and the trial function is well-behaved. In the case where $V'(x_p) = 0$, however, $\eta'(x_t)$ goes to zero and the trial function diverges.

ACKNOWLEDGMENT

The corresponding author would like to acknowledge support by the 2013 Sabbatical Year Research Grant of the University of Seoul. The authors would also like to thank the reviewers for their helpful remarks, as well as Byung-Gon Kim for useful technical discussion.

REFERENCES

1. M. J. Adams, *An Introduction to Optical Waveguides* (New York, USA, Wiley, 1981), Chapter 5.
2. R. Srivastava, C. K. Kao, and R. V. Ramaswamy, "WKB analysis of planar surface waveguides with truncated index profiles," J. Lightwave Technol. **5**, 1605-1609 (1987).
3. W. Berglund and A. Gopinath, "WKB analysis of bend losses in optical waveguides," J. Lightwave Technol. **18**, 1161-1166 (2000).
4. R. E. Langer, "On the asymptotic solutions of ordinary differential equations, with an application to the Bessel functions of large order," Trans. Amer. Math. Soc. **33**, 23-64 (1931).
5. I. C. Goyal, R. Jindal, and A. K. Ghatak, "Planar optical waveguides with arbitrary index profile: An accurate method of analysis," J. Lightwave Technol. **15**, 2179-2182 (1997).
6. S. Roy, A. K. Ghatak, I. C. Goyal, and R. L. Gallawa, "Modified Airy function method for the analysis of tunneling problems in optical waveguides and quantum-well structures," IEEE J. Quantum Electron. **29**, 340-345 (1993).
7. M. S. Chung and C.-M. Kim, "General eigenvalue equations for optical planar waveguide with arbitrarily graded index profile," J. Lightwave Technol. **18**, 878-885 (2000).
8. J.-H Pi, K.-T. Lee, D. Park, and C.-M. Kim, "Analysis of graded-index Hollow optical fibers and its application to atomic waveguide design," J. Lightwave Technol. **28**, 2674-2680 (2010).
9. K.-T. Lee, E. J. Jung, C. H. Kim, and C.-M. Kim, "Derivation of tunneling probabilities for arbitrarily graded potential barriers using modified Airy functions," Optical & Quantum Electronics **42**, 129-141 (2011).
10. K.-T. Lee, E. J. Jung, C. H. Kim, and C.-M. Kim, "Erratum to: Derivation of tunneling probabilities for arbitrarily graded potential barriers using modified Airy functions," Optical & Quantum Electronics **46**, 975-976 (2014).
11. J. Kimeu, R. Mai, and K. Majumdar, "Application of the variational R-matrix method to one-dimensional quantum tunneling," arXiv:quant-ph/0407249v1 (2008).
12. P. K. Mahhapatra, P. Panchadhyayee, S. P. Bhattacharya, and A. Khan, "Resonant tunneling in electrically biased multibarrier systems," Physica B **403**, 2780-2788 (2008).
13. M. Abramowitz and J. A. Stegun, *Handbook of Mathematical Functions*: Nat. Bureau of Standards, 446-447 (1970).